The Journal of Chemical Physics

Dimensionality dependence of the Kauzmann temperature: A case study using bulk and confined water

Cite as: J. Chem. Phys. **154**, 164510 (2021); https://doi.org/10.1063/5.0047656
Submitted: 15 February 2021 . Accepted: 08 April 2021 . Published Online: 28 April 2021

Mohd Moid, Srikanth Sastry, Chandan Dasgupta, Tod A. Pascal, and Prabal K. Maiti

The Journal of Chemical Physics ARTICLE scitation.org/journal/jcp

Dimensionality dependence of the Kauzmann temperature: A case study using bulk and confined water

Cite as: J. Chem. Phys. 154, 164510 (2021); doi: 10.1063/5.0047656
Submitted: 15 February 2021 • Accepted: 8 April 2021 •
Published Online: 28 April 2021

Mohd Moid,[1] Srikanth Sastry,[2] Chandan Dasgupta,[1] Tod A. Pascal,[3] and Prabal K. Maiti[1,a)]

AFFILIATIONS

[1] Department of Physics, Centre for Condensed Matter Theory, Indian Institute of Science, Bangalore 560012, India
[2] Jawaharlal Nehru Centre for Advanced Scientific Research, Bangalore 560064, India
[3] Department of Nanoengineering and Chemical Engineering, University of California San Diego, La Jolla, California 92023, USA

Note: This paper is part of the JCP Special Topic on Fluids in Nanopores.
[a)] **Author to whom correspondence should be addressed:** maiti@iisc.ac.in

ABSTRACT

The Kauzmann temperature (T_K) of a supercooled liquid is defined as the temperature at which the liquid entropy becomes equal to that of the crystal. The excess entropy, the difference between liquid and crystal entropies, is routinely used as a measure of the *configurational entropy*, whose vanishing signals the thermodynamic glass transition. The existence of the thermodynamic glass transition is a widely studied subject, and of particular recent interest is the role of dimensionality in determining the presence of a glass transition at a finite temperature. The glass transition in water has been investigated intensely and is challenging as the experimental glass transition appears to occur at a temperature where the metastable liquid is strongly prone to crystallization and is not stable. To understand the dimensionality dependence of the Kauzmann temperature in water, we study computationally bulk water (three-dimensions), water confined in the slit pore of the graphene sheet (two-dimensions), and water confined in the pore of the carbon nanotube of chirality (11,11) having a diameter of 14.9 Å (one-dimension), which is the lowest diameter where amorphous water does not always crystallize into nanotube ice in the supercooled region. Using molecular dynamics simulations, we compute the entropy of water in bulk and under reduced dimensional nanoscale confinement to investigate the variation of the Kauzmann temperature with dimension. We obtain a value of T_K (133 K) for bulk water in good agreement with experiments [136 K (C. A. Angell, Science **319**, 582–587 (2008) and K. Amann-Winkel *et al.*, Proc. Natl. Acad. Sci. U. S. A. **110**, 17720–17725 (2013)]. However, for confined water, in two-dimensions and one-dimension, we find that there is no finite temperature Kauzmann point (in other words, the Kauzmann temperature is 0 K). Analysis of the fluidicity factor, a measure of anharmonicity in the oscillation of normal modes, reveals that the Kauzmann temperature can also be computed from the difference in the fluidicity factor between amorphous and ice phases.

I. INTRODUCTION

Water is the most abundant liquid on the planet and plays an important role in determining properties of interest in diverse contexts. It is also a liquid with a wide range of peculiar, or *anomalous*, properties, which have been widely studied. Of particular interest have been the properties of amorphous solid phases—water exhibits at least two clearly distinguishable amorphous phases, the low density and high density amorphous solid forms, which are now understood to be associated with the presence of a liquid–liquid transition. Investigating the glass transition[1–4] in water experimentally has been challenging as it appears to occur in a temperature range where the supercooled liquid is not stable with respect to crystallization, the so-called *no man's land*.[6,8–10] The glass transition in water is generally believed to occur at around T = 136 K, and the highly viscous liquid has been observed in a narrow temperature range up to ~150 to 160 K above which it rapidly crystallizes.[5,13–15] Although liquid water in computer simulations does not

crystallize as readily, simulating water in the relevant temperature range is challenging[22] because of the extremely slow dynamics.[23] Water is also expected to display a fragile-to-strong crossover in the temperature dependence of its relaxation dynamics (associated with the so-called "Widom line"), which makes extrapolations from higher temperature behavior difficult. Nevertheless, computer simulations have been employed to characterize both the crossover in behavior around 200 K and the glass transition around 136 K.[22]

There has been considerable interest in studying water under conditions of confinement[20,21] for a variety of reasons, including the fact that water in biological environments often occurs under strongly confined conditions. Such confinement affects the dynamics of water strongly and may correspondingly be expected to influence the glass transition behavior. Water (or other liquids) in confinement corresponds to realizations of liquids in effectively lower spatial dimensions, and thus, their study also is directly relevant to how spatial dimensionality affects glass transition behavior. In particular, whether a finite thermodynamic glass transition exists in dimensions less than three has recently been addressed. We address this question by studying thermodynamic aspects of bulk water, alongside water in two- and one-dimensional confinements. In particular, we study the excess entropy of liquid (or amorphous) water and evaluate the Kauzmann temperature.

In 1948, Kauzmann calculated the difference between the entropy of liquid and crystal phases, the excess entropy, as a function of temperature and reported that the excess entropy decreases rapidly with temperature in the supercooled region.[11,16–18] By extrapolation, the excess entropy was shown to vanish at a finite temperature for a variety of substances, an intriguing observation referred to as the Kauzmann paradox. The temperature at which the extrapolated excess entropy vanishes,

$$\Delta S(T_K) = S_{liq}(T_K) - S_{cry}(T_K) = 0, \tag{1}$$

is termed as the Kauzmann temperature. Kauzmann proposed that a supercooled liquid would go through a glass transition above the temperature where liquid entropy becomes equal to the crystal entropy as one possible resolution of the Kauzmann paradox. Subsequent research associates the vanishing of the excess entropy (or, more appropriately, the *configurational* entropy) as a marker of a thermodynamic glass transition. The excess entropy is routinely employed as an estimate of the glass transition temperature. Experimentally, the Kauzmann temperature has been estimated to be around 136 K,[12,16,17] which is ~1/2 of the melting temperature, T_M (273 K), at variance with typical glass formers, and the significance of this lowered value of the glass transition has been analyzed.[22]

To investigate the role of confinement on the glass transition in water, we compute the excess entropy of bulk water, water confined in two-dimensional geometry, between graphene sheets, and in one-dimensional confinement, within carbon nanotube. The entropies of ice and amorphous phases are evaluated using the 2PT procedure.[44,62] For bulk water, we estimate the Kauzmann temperature around 136 K, and we observe a crossover in the behavior of the excess entropy around 200 K, consistent with previous work. In contrast, in one- and two-dimensional confinement, we find the excess entropies to be small at all temperatures (comparable to the values in the temperature range below 200 K for bulk water) but remain finite at all finite temperatures. Thus, our investigation reveals that there exists no finite Kauzmann temperature for confined water. The conclusions drawn from the study of excess entropy are corroborated by the behavior of *fluidicity*, a quantity that characterizes the fluid-like component of the estimated entropy in the 2PT method.

II. MD SIMULATION DETAILS

Atomistic molecular dynamics (MD) simulations were performed for bulk and confined water by using TIP4P-2005f, a flexible version of the TIP4P-2005 water model,[25] which is known to reproduce various water properties very accurately over a wide range of temperatures.[26,29,30] Most of the results for the TIP4P-2005f model are in line with its rigid predecessor,[49] with a 4° improvement in melting temperature (254 K). Although the melting temperature of the TIP4P-2005 water model (250 K) is ~23 K lesser than the experimental value (273 K), the glass transition temperature calculated by Saito and Bagchi[27] (135 K) agrees very well with the experimental value (136 K).[12,16,17,52]

Simulation was performed for bulk water in the amorphous (liquid) phase and hexagonal ice phase in three-dimensions (henceforth referred to as 3D) and amorphous water and ice confined inside the graphene slit pore (henceforth referred to as 2D) and inside the channel of the CNT of chirality (11,11) (henceforth referred to as 1D). The initial configurations of ice phases of water are shown in Fig. 1. MD simulation was performed for hexagonal ice of 432 water molecules at 5 K in the NPT ensemble. After 50 ns NPT simulation, the final configuration from a 5 K temperature run was used as input to the next higher temperature of 100 K and so on. This sequential heating protocol was followed by other simulations at 100, 140, 170, 230, and 270 K. NVT simulations were performed for 50 ns using the equilibrated density in the NPT ensemble. Another

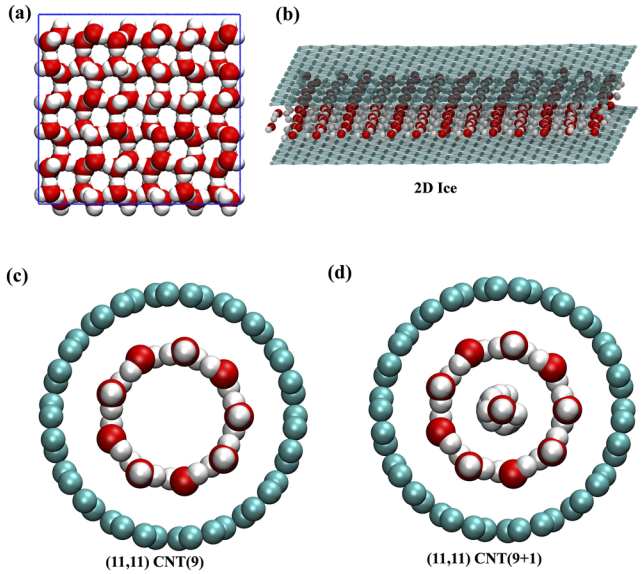

FIG. 1. Initial ice structure for (a) bulk hexagonal ice, (b) two-dimensional square ice inside the graphene slit pore, (c) nonagon ice (9 chain), and (d) nonagon ice with a central chain (9+1 chain) inside the CNT of chirality (11,11).

set of 500 water molecules was cooled from 300 to 5 K through the temperature 280, 275, 270, 250, 240, 235, 230, 225, 222, 220, 215, 205, 202, 197, 190, 180, 170, 160, 150, 145, 135, 130, 125, 120, 110, 100, and 5 K. Here, we applied a sequential cooling protocol, where the final configuration from a particular temperature run was used as input to the next lower temperature. Simulations of length 100 ns, 250 ns, and 500 ns were run for temperatures above 220 K, from 220 to 180 K, and below 180 K, respectively, which was followed by a 10 ns NVT run. The velocity-rescale[28] thermostat and Parrinello–Rahman barostat were used in NPT simulation with 1.3 ps and 2.3 ps coupling constants, respectively. The calculated density of bulk water as a function of temperature is plotted in the upper panel of Fig. 2 and is found to be in good agreement with reported results in the literature.[22,49]

We also performed simulations with the CNT of chirality (11,11) and a 4×4 nm^2 graphene nanoslit pore embedded in a water bath. Snapshots of the initial ice structures inside the (11,11) CNT and the graphene nanoslit pore are shown in Fig. 1. The initial structures were constructed based on previously reported structures.[31–34] These ice structures inside single walled CNTs are varied[31–37] and depend strongly on the CNT diameter. They may comprise either an empty ice shell (ice nanotubes) or an ice shell wrapping a central single file water chain along the axis of the CNT (Fig. 1). For the 2D Ice structure, we chose the recently reported "square-ice" motif.[38–41] We initiated each ice simulation at 5 K with the initial ice structures solvated in a water box with 15 Å water layers in all the three directions. We performed the initial conjugate gradient energy minimization to remove bad contacts. Three sets of simulations were performed for square ice, nonagon ice, and nonagon ice with a central chain at 5, 30, 60, 100, 140, 170, 200, 230, 270, and 300 K using the sequential heating protocol. In each case, we performed 40 ns NPT simulation followed by a 10 ns NVT run. For the amorphous phase, another set of simulations was performed for the CNT and graphene nanoslit pore embedded in a bath of water. We cooled the system, starting from 400 K, in a 10 K interval per 40 ns NPT simulation using the sequential cooling protocol down to 10 K, followed by 10 ns NVT simulation. The graphene slit-pore and CNT were restrained throughout the simulation using the harmonic restraint with a spring constant of 1000 (kJ/mol)/nm^2. The total number of water molecules in the square-ice system is 5108 (water molecules in the bath are also included). Similarly, nanotube-ice systems (including the bath waters) have 4383 and 4433 molecules for nonagon ice and nonagon ice with a central chain, respectively. For the amorphous case, simulated systems had 5013 and 3989 water molecules for the graphene nanoslit and (11,11) CNT, respectively. After 10 ns NVT simulation, additional sets of NVT simulations of 100 ps were performed, with the trajectory (atomic positions and velocities) saved at every 2 fs interval. The entropy was then computed from post-trajectory analysis using an in-house code that implements the 2PT method. The reported values were obtained from statistical averaging over 5 independent sets of trajectories, similar to our previous studies on confined water.[24,37,42,43]

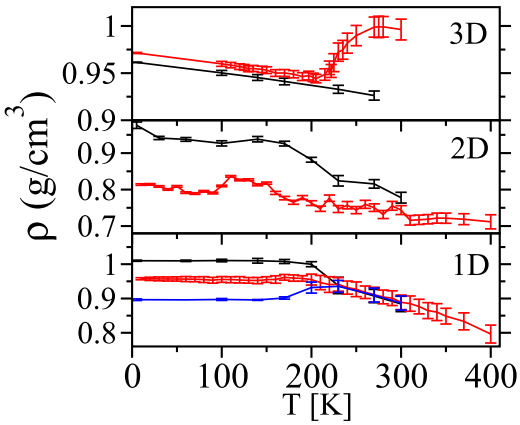

FIG. 2. Temperature dependence of density for the bulk phase (upper panel) of water while lowering the temperature from 300 to 5 K (red) and heating the hexagonal ice from 5 to 270 K (black), (middle panel) density of water, inside the graphene slit pore, which forms square-ice (black) and 2D amorphous (red) phases, and finally (lower panel) density of water while lowering the temperature (red) from 400 to 10 K and while raising the temperature for nonagon ice (blue) and nonagon ice with a central chain (black) structured system in the (11,11) CNT.

III. METHOD

The entropy of bulk and confined water molecules was calculated using the Two-Phase Thermodynamics(2PT) method.[44,62] The calculated entropy using the 2PT method quantitatively agrees well with the available experimental results over a wide range of temperature. The 2PT method also gives entropy values in close agreement with values obtained from free energy perturbation (FEP) and other approximating schemes such as finite difference (FD) and nearest-neighbor pair correlation functions (NN) also. In 2PT, one assumes that the thermodynamic properties of liquids can be computed by treating the DOS of a liquid as a sum of solid-like $[g^s(\nu)]$ and gas-like $[g^g(\nu)]$ contributions. Thermodynamic quantities for a solid can be computed by treating its phonon modes as non-interacting harmonic oscillators, as in the Debye model.[45] However, the gas part is described as an exponentially decaying function of a low-density hard-sphere fluid,[45] for which one can compute the DOS analytically.[46,47] Based on the above description, Lin *et al.*[44,62] reported very accurate thermodynamic properties of Lennard-Jones fluids, over a wide range of thermodynamic state points, using the DOS function obtained from only a 20 ps MD trajectory. In the latter work, Lin *et al.*[62] demonstrated that for polyatomic fluids, the decomposition scheme can be implemented to compute the rotational entropy as well. Here, we provide a brief description of the 2PT method. Readers are referred to the original papers[44,62] for further details. In 2PT, the total entropy is written as the sum of various components as follows:

$$S = S^S_{trans} + S^g_{trans} + S^S_{rot} + S^g_{rot} + S_{i-vib}, \quad (2)$$

where S^S_{trans} and S^g_{trans} are the solid-like and gas-like components of translational entropy, respectively; similarly, S^S_{rot} and S^g_{rot} are the solid-like and gas-like components of rotational entropy; and S_{i-vib} is the internal vibrational entropy. The first two terms arise from translational motion, the third and fourth terms are associated with rotational motion, and the last term is associated with internal vibrational motion of the H_2O molecule.

Here, we discuss the translational components of entropy [first and second terms in Eq. (2)]. A similar treatment can be implemented for the rotational and vibrational components of the entropy (details are in Ref. 62).

As discussed above, under the harmonic approximation, the solid-like translational entropy can be defined as

$$S^{S}_{trans} = \int_0^\infty g^{S}(\nu) W^{S}_{HO}(\nu) d\nu, \tag{3}$$

where $g^{S}(\nu)$ is the density of states for nondiffusive solid-like vibrations, which can be computed using Eq. (5) for the atomistic density of states and Eq. (13) for the fluidicity factor f. $W^{S}_{HO}(\nu)$ is the weight function for the entropy of a quantum harmonic oscillator [Eq. (17)].

Similarly, the gas-like translational entropy can be written as

$$S^{g}_{trans} = \int_0^\infty g^{g}(\nu) W^{g}_{HS}(\nu) d\nu, \tag{4}$$

where $g^{g}(\nu)$ is the density of states for gas-like diffusive density of states, which can also be obtained from the decomposition of the density of states and the fluidicity factor f. $W^{g}_{HS}(\nu)$ is the weight function for the entropy of the hard sphere gas [Eq. (18)].

We know that the density of states, $g(\nu)$, can be computed from the Fourier transform of the translational velocity autocorrelation function[44,62]

$$g(\nu) = \frac{2}{k_B T} \sum_{j=1}^{N} \sum_{k=1}^{3} m_j s_j^k(\nu), \tag{5}$$

where m_j is the mass of the jth atom, k denotes the three Cartesian directions, and $s_j^k(\nu)$ are the atomic spectral densities given by the following equation:

$$\begin{aligned} s_j^k(\nu) &= \lim_{\tau\to\infty} \frac{\left|\int_{-\tau}^{\tau} v_j^k(t) e^{-i2\pi\nu t} dt\right|^2}{\int_{-\tau}^{\tau} dt} \\ &= \lim_{\tau\to\infty} \frac{\left|\int_{-\tau}^{\tau} v_j^k(t) e^{-i2\pi\nu t} dt\right|^2}{2\tau}, \end{aligned} \tag{6}$$

where $v_j^k(t)$ is the velocity component in the kth direction of the jth atom. It can be demonstrated that the atomic spectral density, $s_j^k(\nu)$, can be obtained from the Fourier transform of the velocity auto-correlation function (VACF) $c_j^k(t)$,[44]

$$s_j^k(\nu) = \lim_{\tau\to\infty} \int_{-\tau}^{\tau} c_j^k(t) e^{-i2\pi\nu t} dt, \tag{7}$$

where $c_j^k(t)$ is given by

$$c_j^k(t) = \lim_{\tau\to\infty} \frac{1}{2\tau} \int_{-\tau}^{\tau} v_j^k(t+t') v_j^k(t') dt'. \tag{8}$$

Thus, Eq. (5) can be rewritten as

$$g(\nu) = \frac{2}{k_B T} \lim_{\tau\to\infty} \int_{-\tau}^{\tau} \sum_{j=1}^{N} \sum_{k=1}^{3} m_j c_j^k(t) e^{-i2\pi\nu t} dt. \tag{9}$$

More generally, it can be written as

$$g(\nu) = \frac{2}{k_B T} \lim_{\tau\to\infty} \int_{-\tau}^{\tau} C(t) e^{-i2\pi\nu t} dt. \tag{10}$$

In the above equation, $C(t)$ can be either the mass-weighted translational velocity auto-correlation function (VACF) determined from the center of mass velocity $V_i^{cm}(t)$ of the ith molecule,

$$C_T(t) = \sum_{i=1}^{N} \left\langle m_i V_i^{cm}(t) . V_i^{cm}(0) \right\rangle, \tag{11}$$

or the moment-of-inertia weighted angular velocity auto-correlation function

$$C_R(t) = \sum_{i=1}^{3} \sum_{i=1}^{N} \langle I_{ij} \omega_{ij}(t) \omega_{ij}(0) \rangle, \tag{12}$$

where I_{ij} is the moment-of-inertia tensor and ω_{ij} is the angular velocity of the jth component of the ith molecule. Depending on the use of $C_T(t)$ or $C_R(t)$ in Eq. (10), one can obtain the translational or rotational DOS.

Drawing inspiration from an idea of Eyring in his thesis on significant structure theory,[48] Lin *et al.*[44] proposed a self-consistent partitioning factor, denoted as fluidicity factor f, based solely on the system's diffusivity compared to a gas of hard spheres at the same density and temperature. The DOS is decomposed into a solid-like non-diffusive component and a gas-like diffusive component, $g(\nu) = g^{S}(\nu) + g^{g}(\nu)$, using the fluidity factor f, which is a measure of the fluidity of a system. f is calculated in terms of the dimensionless diffusivity Δ using the universal equation[44]

$$2\Delta^{-9/2} f^{15/2} - 6\Delta^{-3} f^{5} - \Delta^{-3/2} f^{7/2} + 6\Delta^{-3/2} f^{5/2} + 2f - 2 = 0. \tag{13}$$

The hard sphere diffusivity, Δ, can be uniquely determined for a thermodynamic state of the system using the following equation:

$$\Delta(T, \rho, m, g_0) = \frac{2 g_0}{9N} \left(\frac{6}{\pi}\right)^{2/3} \left(\frac{\pi k_B T}{m}\right)^{1/2} \rho^{1/3}, \tag{14}$$

where $g_0 = g(0)$ is the zero-frequency component of the DOS function (translational or rotational). Obtaining f from Eqs. (13) and (14), the gas-like diffusive component of the DOS can be obtained using a hard-sphere diffusive model,

$$g^{g}(\nu) = \frac{g_0}{1 + \left[\frac{\pi g_0 \nu}{6fN}\right]^2}. \tag{15}$$

Lin *et al.*[62] employed the gas–solid decomposition scheme for rotational entropy as well.[62] They demonstrated that for polyatomic fluids, the decomposition scheme can be implemented on rotational motion with a different fluidity factor (f) based on the rotational diffusivity in Eq. (10). Then, the gas-like components of entropy, also known as configurational entropy (S_{conf}), are calculated using Eq. (15) with g_0 being $g_{tran}(0)$ or $g_{rot}(0)$ for the translational and rotational cases, respectively. Given such a decomposition of DOS, one can compute any thermodynamic quantity A_m from the solid-like and gas-like DOS functions with the corresponding weight functions as follows.

$$A_m = \beta^{-1} \left[\int_0^\infty g_m^{g}(\nu) W_{A,m}^{g} d\nu + \int_0^\infty g_m^{s}(\nu) W_{A,m}^{s} d\nu \right], \tag{16}$$

where m stands for translational, rotational, or vibrational motion. The weight function for entropy is defined as

TABLE I. Density (in g/cc) of bulk and confined water for all the systems studied in this work.

Temperature (K)	3D (ice)	3D (amorphous)	2D (ice)	2D (amorphous)	1D (9 chain ice)	1D (9+1 chain ice)	1D (amorphous)
5 K	0.9614 ± 0.0002	0.9714 ± 0.0006	0.9764 ± 0.0089	⋯	0.8965 ± 0.0022	1.0101 ± 0.0017	⋯
10 K	⋯	⋯	⋯	0.8138 ± 0.0022	⋯	⋯	0.9576 ± 0.0031
20 K	⋯	⋯	⋯	0.8142 ± 0.0022	⋯	⋯	0.9573 ± 0.0047
30 K	⋯	⋯	0.9414 ± 0.0044	0.8086 ± 0.0021	0.8964 ± 0.0000	1.0100 ± 0.0000	0.9572 ± 0.0056
40 K	⋯	⋯	⋯	0.8002 ± 0.0020	⋯	⋯	0.9568 ± 0.0061
50 K	⋯	⋯	⋯	0.8089 ± 0.0022	⋯	⋯	0.9569 ± 0.0062
60 K	⋯	⋯	0.9375 ± 0.0051	0.7916 ± 0.0022	0.8960 ± 0.0000	1.0099 ± 0.0020	0.9567 ± 0.0074
70 K	⋯	⋯	⋯	0.7891 ± 0.0022	⋯	⋯	0.9560 ± 0.0073
80 K	⋯	⋯	⋯	0.7953 ± 0.0022	⋯	⋯	0.9551 ± 0.0085
90 K	⋯	⋯	⋯	0.7906 ± 0.0023	⋯	⋯	0.9532 ± 0.0084
100 K	0.9502 ± 0.0026	0.9598 ± 0.0026	0.9266 ± 0.0071	0.8099 ± 0.0021	0.8971 ± 0.0028	1.0107 ± 0.0038	0.9556 ± 0.0084
110 K	⋯	0.9585 ± 0.0028	⋯	0.8363 ± 0.0021	⋯	⋯	0.9547 ± 0.0087
120 K	⋯	0.9569 ± 0.0030	⋯	0.8262 ± 0.0023	⋯	⋯	0.9546 ± 0.0093
125 K	⋯	0.9561 ± 0.0030	⋯	⋯	⋯	⋯	⋯
130 K	⋯	0.9546 ± 0.0031	⋯	0.8268 ± 0.0026	⋯	⋯	0.9528 ± 0.0083
135 K	⋯	0.9550 ± 0.0032	⋯	⋯	⋯	⋯	⋯
140 K	0.9453 ± 0.0031	⋯	0.9381 ± 0.0074	0.8129 ± 0.0026	0.8957 ± 0.0012	1.0101 ± 0.0069	0.9522 ± 0.0090
145 K	⋯	0.9540 ± 0.0033	⋯	⋯	⋯	⋯	⋯
150 K	⋯	0.9531 ± 0.0036	⋯	0.8176 ± 0.0029	⋯	⋯	0.9552 ± 0.0082
160 K	⋯	0.9501 ± 0.0036	⋯	0.7909 ± 0.0042	⋯	⋯	0.9554 ± 0.0109
170 K	0.9411 ± 0.0035	0.9501 ± 0.0037	0.9260 ± 0.0065	0.7766 ± 0.0046	0.9014 ± 0.0033	1.0079 ± 0.0058	0.9618 ± 0.0082
180 K	⋯	0.9486 ± 0.0038	⋯	0.7651 ± 0.0054	⋯	⋯	0.9596 ± 0.0092
190 K	⋯	0.9463 ± 0.0041	⋯	0.7781 ± 0.0054	⋯	⋯	0.9584 ± 0.0080
197 K	⋯	0.9474 ± 0.0047	⋯	⋯	⋯	⋯	⋯
200 K		⋯	0.8817 ± 0.0066	0.7630 ± 0.0065	0.9319 ± 0.0161	0.9999 ± 0.0073	0.9551 ± 0.0159
202 K	⋯	0.9455 ± 0.0045	⋯	⋯	⋯	⋯	⋯
205 K	⋯	0.9442 ± 0.0045	⋯	⋯	⋯	⋯	⋯
210 K	⋯	⋯	⋯	0.7475 ± 0.0072	⋯	⋯	0.9465 ± 0.0208
215 K	⋯	0.9485 ± 0.0061	⋯	⋯	⋯	⋯	⋯
220 K	⋯	0.9556 ± 0.0072	⋯	0.7763 ± 0.0088	⋯	⋯	0.9406 ± 0.0229
222 K	⋯	0.9523 ± 0.0069	⋯	⋯	⋯	⋯	⋯
225 K	⋯	0.9611 ± 0.0095	⋯	⋯	⋯	⋯	⋯
230 K	0.9328 ± 0.0043	0.9723 ± 0.0097	0.8241 ± 0.0143	0.7467 ± 0.0095	0.9353 ± 0.0174	0.9379 ± 0.0238	0.9413 ± 0.0199
235 K	⋯	0.9747 ± 0.0100	⋯	⋯	⋯	⋯	⋯
240 K	⋯	0.9818 ± 0.0106	⋯	0.7572 ± 0.0100	⋯	⋯	0.9318 ± 0.0191
250 K	⋯	0.9898 ± 0.0107	⋯	0.7437 ± 0.0098	⋯	⋯	0.9268 ± 0.0215
260 K	⋯	⋯	⋯	0.7595 ± 0.0110	⋯	⋯	0.9181 ± 0.0182
270 K	0.9262 ± 0.0048	0.9898 ± 0.0107	0.8157 ± 0.0116	0.7505 ± 0.0104	0.9098 ± 0.0205	0.9071 ± 0.0194	0.9111 ± 0.0216
275 K	⋯	0.9990 ± 0.0113	⋯	⋯	⋯	⋯	⋯
280 K	⋯	0.9991 ± 0.0109	⋯	0.7316 ± 0.0111	⋯	⋯	0.9044 ± 0.0201
290 K	⋯	⋯	⋯	0.7554 ± 0.0121	⋯	⋯	0.9009 ± 0.0215
300 K	⋯	0.9962 ± 0.0110	0.7778 ± 0.0147	0.7438 ± 0.0122	0.8867 ± 0.0205	0.8841 ± 0.0224	0.8888 ± 0.0212
310 K	⋯	⋯	⋯	0.7158 ± 0.0130	⋯	⋯	0.8851 ± 0.0222
320 K	⋯	⋯	⋯	0.7173 ± 0.0129	⋯	⋯	0.8764 ± 0.0214
330 K	⋯	⋯	⋯	0.7187 ± 0.0127	⋯	⋯	0.8646 ± 0.0233
340 K	⋯	⋯	⋯	0.7218 ± 0.0137	⋯	⋯	0.8603 ± 0.0247
350 K	⋯	⋯	⋯	0.7216 ± 0.0139	⋯	⋯	0.8485 ± 0.0229
370 K	⋯	⋯	⋯	0.7188 ± 0.0149	⋯	⋯	0.8332 ± 0.0247
400 K	⋯	⋯	⋯	0.7116 ± 0.0194	⋯	⋯	0.7962 ± 0.0261

$$W^{S}_{A,m}(\nu) = W^{HO}_{S}(\nu) = \frac{\beta\hbar\nu}{\exp(\beta\hbar\nu) - 1} - \ln[1 - \exp(-\beta\hbar\nu)], \quad (17)$$

where $\beta = 1/kT$ and $\hbar$ is Plank's constant,

$$W^{g}_{A,m}(\nu) = W^{HS}_{g}(\nu) = \frac{1}{3}\frac{S^{HS}}{k}. \quad (18)$$

Thus, it is axiomatic that the total entropy depends on the frequencies and fluidicity factors (f_s) associated with various motions. Using this method, several water models have been found to yield very accurate results for thermodynamic quantities over a wide range of thermodynamic state points. Above all, this method converges for a small MD trajectory (20 ps).

IV. RESULTS

A. Bulk water

The temperature dependence of density of the bulk phase (3D) is plotted in the upper panel of Fig. 2. While decreasing the temperature from 300 to 5 K, the density profile first increases and attains global maximum at 280 K in good agreement with the findings of Miguel and Abascal[49] and very close to the experimental value of 277 K. After this point, the density gradually decreases until 205 K, where it achieves a global minimum. This is followed by another region of increasing density until 5 K. We find that between the global maximum and minimum, the density profile changes the slope near 230 K with an inflection point near 220 K. Taken together, the non-monotonic temperature profile suggests structural or dynamical crossover near 205, 230, and 280 K. The values of the density at different temperatures have been tabulated in Table I.

Figure 3 (upper panel for 3D) shows the DOS of bulk water in the amorphous and hexagonal ice phases at 170 and 270 K. We further decompose the total DOS into contributions arising from molecular center of mass diffusion ($DOS_{diffuse}$), librational, low frequency rattling modes as in a solid ($DOS_{lib-trans}$), (hindered) rotations about the center of mass (DOS_{rot}), and internal molecular vibrations (DOS_{i-vib}). Analysis of the $DOS_{lib-trans}$ spectrum (which extends up to ~350 cm^{-1}) reveals two peaks at ~50 and ~280 cm^{-1}, which are commonly assigned to inter-molecular hydrogen bond (HB) bending and HB stretching motions, respectively.[27,50] We find that the $DOS_{lib-trans}$ peak for the HB stretching motion in the amorphous phase appears at a lower energy than that of the hexagonal ice phase at the same temperature, suggesting a more diverse HB environment in the amorphous phase and an overall shallower potential. Moreover, we find that in both cases, the energy of the HB-stretching mode red shifts to a lower frequency with decreasing temperature by ~20 cm^{-1} over 100 K. Between 350 and 1100 cm^{-1}, there is a broad band arising from rotational libration motion. With increasing the temperature, the line shape of this band increases in width and starts to overlap with the translational–librational bands, leading to highly coupled molecular motions near 270 K. Above 1500 cm^{-1}, there are two peaks at ~1670 and ~3300 cm^{-1} emerging from intra-molecular H–O–H angle bending and –OH stretching motions, respectively. With increasing temperature, we find that the HOH bending mode red shifts while the –OH stretching mode blueshifts, reflecting changes in the HB network due to a change in the external potential brought on by structural transformations. Overall, these changes in the DOS result in entropic signatures of the amorphous and hexagonal ice phases, as discussed in Sec. IV A 1.

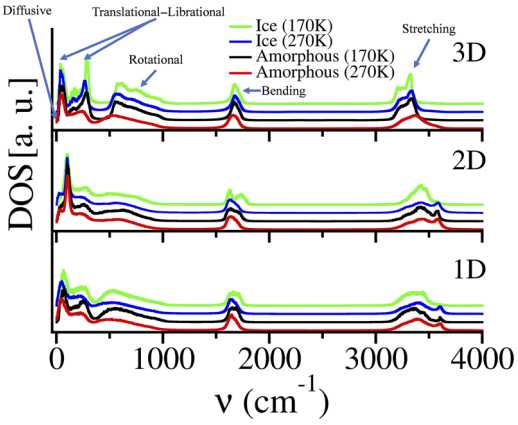

FIG. 3. Density of states of bulk water (upper panel), water confined inside the graphene slit-pore (middle panel), and water confined inside the (11,11) CNT at 170 and 270 K. For all the temperatures, the DOS has been plotted for all the systems which was, starting from ice and the amorphous phase, studied in this work. The DOS is shifted on the Y axis for clarity.

1. Determination of Kauzmann temperature from total entropy

The Kauzmann temperature depends on the entropy difference between ice and amorphous phases of the system, which we computed accurately using the 2PT method over a wide range of temperatures. The entropy of water calculated with the 2PT method employing quantum correction has been shown to be consistent with reported values using the quantum corrected specific heat[27] for the TIP4P-2005 water model.[51] Note that for most of the liquids, quantum effects on entropy become relevant only at low temperatures, specifically below 100 K. However, for water, quantum effects are known to be important even at room temperature due to the high frequency intra- and inter-molecular vibrations and the complex HB network, as discussed in Sec. IV A. For bulk water, we find that the total entropy of the bulk liquid (or the amorphous solid) is always greater than that of the hexagonal ice phase (left panel of Fig. 4 and Table II). Furthermore, by decomposing the total entropy into components arising from the various molecular vibrational motions, we show that the translational entropy is always higher than the rotational and vibrational components over the entire temperature range investigated. This is expected as the translational modes have the lowest frequency. Thus, the distinguishing entropic signature of amorphous ice is its relatively large translational entropy above 200 K, compared to hexagonal ice (left panel of Fig. 5). The entropic difference between these two phases decreases rapidly between 270 and 200 K (left panel of Fig. 6) due to large scale density fluctuations, whereas below 200 K, more muted fluctuations result in smaller entropic differences. In Fig. 6 (left panel), we plot the entropy difference [ΔS, defined in Eq. (1)] between the amorphous and ice phases of the system. A linear fit of the entropy difference, ΔS, above 205 K and between 150 and 205 K, crosses zero at 199 K and 133 ± 50 K,

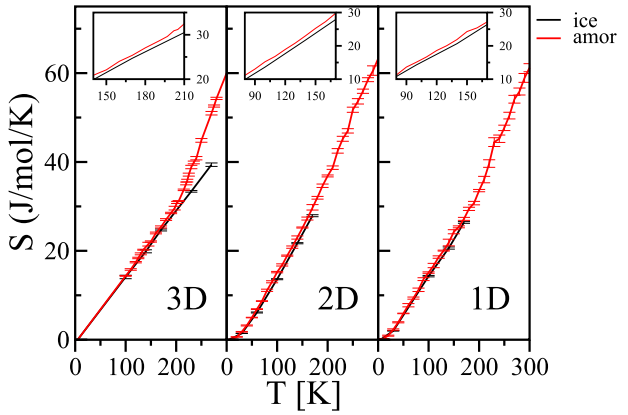

FIG. 4. Entropy of the bulk water (left panel) in the hexagonal ice phase (black) and amorphous phase (red); entropy of water in the square-ice (black) and 2D amorphous (red) phase as a function of temperature inside the graphene slit nanopore (middle panel); and entropy of water in nonagon ice with a central chain (black) and amorphous (red) as a function of temperature inside the (11,11) CNT (right panel). In all the cases, the entropy in the amorphous phase is higher than that of ice, including the error bars (numbers are provided in Table II) over a wide temperature range. Insets are the zoomed image of the plots to demonstrate the entropy difference at low temperature in each panel.

respectively (left panel of Fig. 6), which thus defines the Kauzmann temperature of bulk water to be 133 K. This calculated T_K is close to the experimental value of the glass transition temperature,[12,52] T_g = 136 K, for the low density liquid, and agrees well with the simulation study by Saito and Bagchi, where they reported T_K = 135 K.[27] Note that the value of T_g for the high density liquid is 116 K.[52] Other experiments have reported a T_g of 124 K without annealing[53] and 113–148 K for hyperquenched water.[17]

2. Determination of Kauzmann temperature from fluidicity factors

We now propose another way to determine the Kauzmann temperature using the fluidicity factor introduced in Sec. III. We plot the fluidicity factor for translational and rotational components in various phases (in the left panel of Fig. 7). The rotational component of entropy does not contribute significantly to the total entropy difference at a low temperature range. Hence, similar to the total entropy as discussed in Sec. IV A 1, we also plot the difference between the fluidicity factor of the ice phase and amorphous phase for the translational (Δf_{trans}) degree of freedom (in the left panel of Fig. 8). Linear fits of the difference in the translational fluidicity factors, Δf_{trans}, above 205 K and between 150 and 205 K, cross zero at 213 K and 150 ± 67 K, respectively. The difference in the fluidicity factor (Δf) overpredicts, compared to the values obtained using total entropy, the fragile-to-strong transition temperature[19] as well as the Kauzmann temperature, T_K. The frequency shift between two states of matter (water) is featured in over-prediction of the dynamical transition temperatures computed by this method.

As demonstrated in Fig. 3, there is a red shift of the rotational–librational band of amorphous ice, indicating a weakening of the covalent bond, strengthening of the HB,[54] and reduced rotational motions. The weakening or strengthening of the HB network is coupled to structural changes with temperature. We find that while the position of the first, second, and fourth peaks of the radial distribution function (upper panel of Fig. 10) shifts toward shorter distance, and concomitantly increases in intensity, with decreasing temperature, the position of the third peak remains relatively unchanged. Here, we interpret these shifts to the increase in the tetrahedral order[55] with decreasing temperature. Moreover, the increase in the first peak intensity with decreasing temperature indicates a more structured first solvation shell, while the area under the second peak is related to the order parameter of liquid–liquid phase transitions[56] between the high density liquid (HDL) and low density liquid (LDL). In the HDL, the second solvation shell is poorly defined due to the presence of interstitial molecules between the first and second coordination shells. On the other hand, the LDL is characterized by well-separated first and second peaks and more ice-like local order in the supercooled liquid.

B. Water under 2D confinement

The density of water molecules confined inside a graphene nano-slit (GNS) is reported in the middle panel of Fig. 2. Upon heating (black line), we find that the density of the 2D square-ice system is constant up to 170 K, followed by a gradual decrease up to 230 K and a convergence to the amorphous density at 300 K. Moreover, we find that the density of the 2D amorphous system increases with decreasing temperature until 110 K, followed by a jump around 100 K, then remains constant until 10 K (red line).

The middle panel of Fig. 3 shows the corresponding DOS functions at 170 and 270 K. Unlike the bulk case, we find a single sharp peak at ~100 cm^{-1} in the $DOS_{lib-trans}$ spectrum with a shoulder at ~260 cm^{-1} arising from inter-molecular hydrogen bond (HB) bending and HB stretching motion, respectively. The HB bending feature is blueshifted compare to its bulk counterpart (~50 cm^{-1}). Most importantly, and in sharp contrast to the bulk, we find that the peak energy and intensity are relatively unaffected by changes in the temperature. Indeed, it is noteworthy that there is a 5 cm^{-1} shift between the peaks of ice and amorphous phases around 100 cm^{-1}, which lies in the region of translational motion.

1. Determination of Kauzmann temperature from total entropy

Considering the thermodynamic properties of the 2D confined liquid, we find that the total entropy in the amorphous phase is slightly greater than that in the 2D square-ice phase. Decomposition of the total entropy into the independent molecular motions shows that the translational and rotational entropies in the liquid are substantially larger, whereas the internal vibrational component of entropy is similar to that of 2D ice between 0 and 170 K (middle panel of Fig. 5). A close look into Fig. 4 revealed that the total entropy of the confined liquid is always greater than that of 2D ice across the entire temperature range. The entropic difference between these two phases decreases slowly with decreasing temperature (middle panel of Fig. 6). A linear fit of the entropy difference, ΔS, below 170 K, crosses the Y axis at 0.2377, which is a measure of excess entropy, defined by Kauzmann, at 0 K (middle panel of Fig. 6). This number suggests that the amorphous phase has greater entropy, though very small amount, than that of ice in 2D confinement even at 0 K; thus,

TABLE II. Entropy (in J/mol/K) of bulk and confined water for all the systems studied in this work.

Temperature (K)	3D (ice)	3D (amorphous)	2D (ice)	2D (amorphous)	1D (9 chain ice)	1D (9+1 chain ice)	1D (amorphous)
5 K	0.0074 ± 0.0003	0.011 ± 0.001	0.0080 ± 0.0009	⋯	0.046 ± 0.008	0.026 ± 0.006	⋯
10 K	⋯	⋯	⋯	0.0870 ± 0.006	⋯	⋯	0.21 ± 0.04
20 K	⋯	⋯	⋯	0.62 ± 0.04	⋯	⋯	0.90 ± 0.11
30 K	⋯	⋯	1.41 ± 0.01	1.78 ± 0.07	2.05 ± 0.10	1.99 ± 0.06	2.28 ± 0.16
40 K	⋯	⋯	⋯	3.20 ± 0.10	⋯	⋯	3.91 ± 0.12
50 K	⋯	⋯	⋯	4.98 ± 0.06	⋯	⋯	5.91 ± 0.06
60 K	⋯	⋯	6.12 ± 0.10	6.88 ± 0.09	7.22 ± 0.18	6.91 ± 0.09	7.75 ± 0.36
70 K	⋯	⋯	⋯	8.69 ± 0.07	⋯	⋯	9.36 ± 0.23
80 K	⋯	⋯	⋯	11.11 ± 0.25	⋯	⋯	11.23 ± 0.38
90 K	⋯	⋯	⋯	13.03 ± 0.22	⋯	⋯	13.63 ± 0.31
100 K	14.12 ± 0.39	14.36 ± 0.08	13.61 ± 0.11	15.21 ± 0.15	14.9 ± 0.33	14.29 ± 0.16	15.11 ± 0.16
110 K	⋯	15.81 ± 0.18	⋯	16.82 ± 0.24	⋯	⋯	16.69 ± 0.48
120 K	⋯	17.44 ± 0.15	⋯	18.92 ± 0.12	⋯	⋯	18.60 ± 0.27
125 K	⋯	18.39 ± 0.16	⋯	⋯	⋯	⋯	⋯
130 K	⋯	19.32 ± 0.22	⋯	20.83 ± 0.26	⋯	⋯	20.04 ± 0.10
135 K	⋯	20.25 ± 0.11	⋯	⋯	⋯	⋯	⋯
140 K	19.89 ± 0.35	⋯	21.71 ± 0.12	23.00 ± 0.36	22.33 ± 0.29	20.63 ± 0.24	21.87 ± 0.75
145 K	⋯	21.50 ± 0.42	⋯	⋯	⋯	⋯	⋯
150 K	⋯	22.09 ± 0.14	⋯	25.24 ± 0.11	⋯	⋯	24.29 ± 0.46
160 K	⋯	24.02 ± 0.20	⋯	27.26 ± 0.32	⋯	⋯	25.40 ± 0.21
170 K	24.70 ± 0.22	25.38 ± 0.23	27.90 ± 0.22	29.79 ± 0.61	27.23 ± 0.20	26.38 ± 0.19	27.19 ± 0.21
180 K	⋯	27.04 ± 0.19	⋯	31.94 ± 0.30	⋯	⋯	29.44 ± 0.36
190 K	⋯	28.52 ± 0.15	⋯	34.64 ± 0.38	⋯	⋯	30.73 ± 0.38
197 K	⋯	29.61 ± 0.41	⋯	⋯	⋯	⋯	⋯
200 K	⋯	⋯	34.62 ± 0.21	36.85 ± 0.21	34.41 ± 0.24	32.51 ± 0.52	33.56 ± 0.25
202 K	⋯	30.89 ± 0.23	⋯	⋯	⋯	⋯	⋯
205 K	⋯	31.18 ± 0.11	⋯	⋯	⋯	⋯	⋯
210 K	⋯	⋯	⋯	38.72 ± 0.39	⋯	⋯	36.04 ± 0.72
215 K	⋯	33.73 ± 0.17	⋯	⋯	⋯	⋯	⋯
220 K	⋯	35.16 ± 0.31	⋯	42.49 ± 0.51	⋯	⋯	39.64 ± 0.84
222 K	⋯	35.80 ± 0.30	⋯	⋯	⋯	⋯	⋯
225 K	⋯	37.15 ± 0.32	⋯	⋯	⋯	⋯	⋯
230 K	33.39 ± 0.19	38.86 ± 0.38	⋯	45.21 ± 0.55	⋯	⋯	44.47 ± 0.98
235 K	⋯	39.89 ± 0.30	⋯	⋯	⋯	⋯	⋯
240 K	⋯	40.84 ± 0.37	⋯	47.00 ± 0.48	⋯	⋯	45.23 ± 0.82
250 K	⋯	44.85 ± 0.42	⋯	51.75 ± 0.57	⋯	⋯	47.68 ± 0.60
260 K	⋯	⋯	⋯	53.64 ± 0.60	⋯	⋯	50.44 ± 0.75
270 K	39.39 ± 0.38	50.97 ± 0.39	⋯	55.91 ± 0.47	⋯	⋯	54.12 ± 0.87
275 K	⋯	52.59 ± 0.23	⋯	⋯	⋯	⋯	⋯
280 K	⋯	54.30 ± 0.25	⋯	58.51 ± 0.44	⋯	⋯	55.86 ± 0.78
290 K	⋯	⋯	⋯	60.57 ± 1.06	⋯	⋯	58.92 ± 0.99
300 K	⋯	60.02 ± 0.17	⋯	63.24 ± 0.51	⋯	⋯	61.22 ± 0.90

we defined the Kauzmann temperature for 2D confined water at 0 ± 20 K.

2. Determination of Kauzmann temperature from fluidicity factor

As discussed for the 3D case, another way to compute T_K is the fluidicity factors computed by the 2PT method (middle panel of Fig. 7). A linear fit of the difference in the translational fluidicity factor, Δf, below 170 K, becomes zero at 21 ± 22 K (middle panel of Fig. 8). The difference in the fluidicity factor over predicts, compared to the total entropy method, the Kauzmann temperature from the translational component. Note that the total entropy, S, is computed from the linear combination of fluidicity factors (f_s) with different

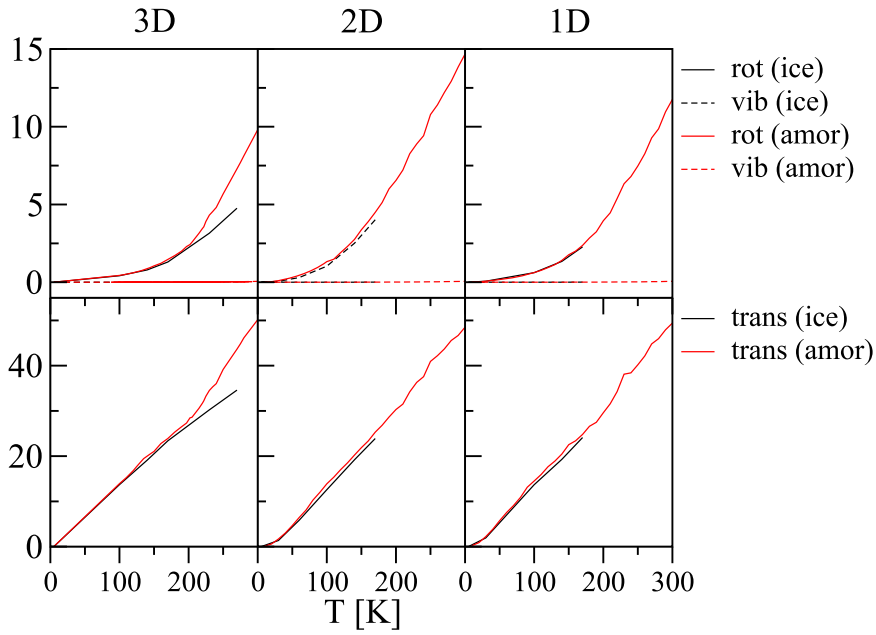

FIG. 5. The decomposition of entropy into rotational and vibrational components (upper panels) and translational component (lower panels) as a function of temperature for various phases of water in different dimensions. The black dashed or full line represents the components in the ice phase, whereas the red dashed or full line represents the same component in the amorphous phase, respectively.

weight functions, which depends on the frequency of oscillation, mass, and moment-of-inertia of the molecule.

The oxygen–oxygen 2D pair correlation function for the square-ice and amorphous structures under 2D nanoconfinement is demonstrated in Fig. 10. We find that for square ice up to 170 K, the 2D RDF is indicative of a well ordered structure, which disappears after melting, between 170 and 230 K. In contrast, the 2D RDF of the amorphous structure, which always has a lower density than the square ice, is indicative of a random structure down to 10 K.

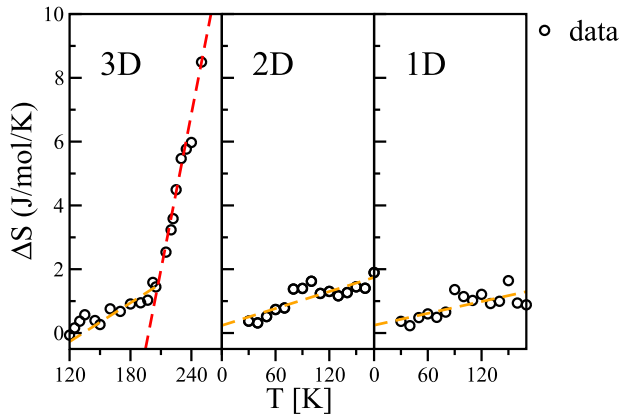

FIG. 6. The entropy difference between the amorphous and the ice phase (black dots denote the data points). Left panel for bulk water: Red and orange lines are the fitting of data above 205 K and between 150 and 205 K, respectively. These lines cross zero at 199 K and 133 K, respectively. The latter one is defined as the Kauzmann temperature, which is very close to the glass transition temperature. Middle panel for water confined inside a graphene slit pore: The orange line is the fitting of the excess entropy data below 170 K. Right panel for water inside the (11,11) CNT: The orange line is the fitting of the excess entropy data below 170 K.

C. Water under 1D confinement

Turning now to water molecules confined inside a (11,11) carbon nanotube (CNT) of diameter 14.9 Å, we find that the density of the amorphous phase (red line in the lower panel of Fig. 2) increases with decreasing temperature and converges to the bulk density in the amorphous phase. The density of nonagon ice with a central chain (black line) is always greater than that of amorphous water (red line), which is greater than nonagon ice until 230 K. Above 230 K, all lines merge into one, which reveals that there exists only one phase. Note that free energy, enthalpy, and entropy calculations (Fig. 9) of these ice structures indicate that nonagon ice with a central chain is more stable than nonagon ice in the (11,11) CNT at low temperatures. The difference in the free energy between the two ice phases is ~10 meV/H_2O, which is equivalent to 120 K. Interestingly, we observed that the Helmholtz free energy in the amorphous phase is lower than both ice phases. The free energy difference between two phases (amorphous and ice) is significant at low temperatures, emerging from the difference in the internal energy. In the amorphous phase, the number of water molecules near the axis of the CNT is higher in percentage compared to ice phases, which provides the stability to the amorphous phase against ice inside the (11,11) CNT.

The lower panel of Fig. 3 shows the DOS of water in the amorphous and nanotube-ice phases confined inside the (11,11) CNT. In both cases, at a fixed temperature, the DOS of water in the nanotube-ice phases is similar to that of the amorphous phase. As the temperature increases, we find that the translational, rotational–librational, and bending mode red shift, while the –OH stretching modes blue shift, similar to the bulk.[57] We find a peak in the translational bands

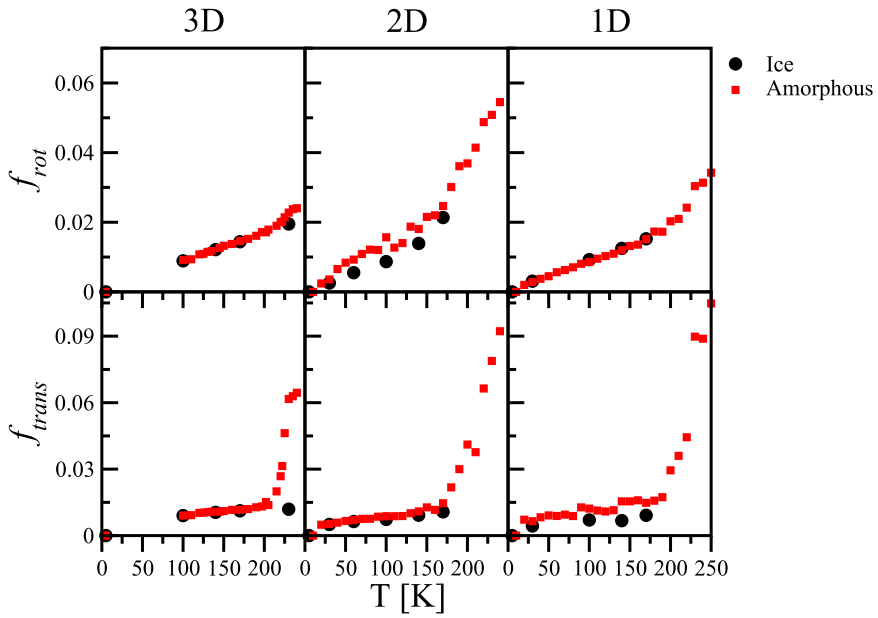

FIG. 7. Fluidicity factors for bulk (left panel), water confined inside the graphene slit pore (middle panel), and water confined inside the (11,11) CNT (right panel). Black dots and red squares denote the fluidicity factors for rotational motion (upper panels) and translational motion (lower panels) in ice and amorphous phases, respectively.

near ~70 cm^{-1} with a shoulder at ~225 cm^{-1} arising from HB bending and stretching motions, respectively. Yet unlike the case of 2D confinement, and similar to the bulk, the bandgap between the translational and rotational–librational modes decreases with increasing temperature for both the ice and amorphous structures. We note that the two stretching modes, arising from the symmetric and asymmetric vibrations of the OH bond, are poorly resolved in bulk but are more distinct under 1D confinement. Additionally, we find the signature of a high energy peak near 3700 cm^{-1}, indicative of broken HBs.[58]

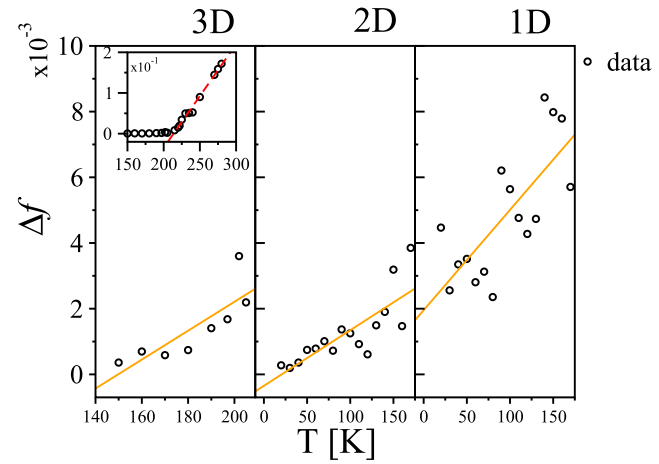

FIG. 8. The difference in the translational fluidicity factor between amorphous and ice phases. The orange line is the linear fit of the data points (left panel) bulk water, (middle panel) water confined in the graphene slit pore (right panel) and water confined in the (11,11) CNT. The inset of the left panel demonstrates the difference in the translational fluidicity factor for the full range of temperature where both 3D phases co-exists.

1. Determination of Kauzmann temperature from total entropy

Consistent with the thermodynamics under 2D nano-confinement, we find that water confined inside the (11,11) CNT has total entropies, in general, greater than that of the ice phases over a temperature range below 170 K. Decomposition of the total into the independent molecular motions further reveals that the difference in the total entropy is arising from the translational component (right panel of Fig. 5). Moreover, the computed difference in entropy between amorphous and ice phases decreases slowly with temperature (right panel of Fig. 6). A linear fit of the entropy difference, ΔS, below 170 K, meets the Y axis at 0.2439 (J/mol)/K (right panel of Fig. 6), which is the difference in the entropy at 0 K. Similar to 2D confinement, this difference reveals that the amorphous phase has higher entropy than the ice phase even at 0 K. Hence we can define the Kauzmann temperature for 1D confined water to be 0 ± 32 K.

2. Determination of Kauzmann temperature from fluidicity factor

As discussed for two other dimensions, we computed T_K from the fluidicity factors as well (right panel of Fig. 7). The linear fit of the difference in the translational fluidicity factors, Δf, below 170 K, crosses the Y axis at 0.002 (right panel of Fig. 8). The difference in the translational fluidicity factor is also non-zero at 0 K, which suggests that the Kauzmann temperature is 0 ± 30 K (orange line in the right panel of Fig. 8).

Further insights into the underlying structural basis for the computed thermodynamics were obtained from the oxygen–oxygen cylindrical distribution function,[59] which is defined as

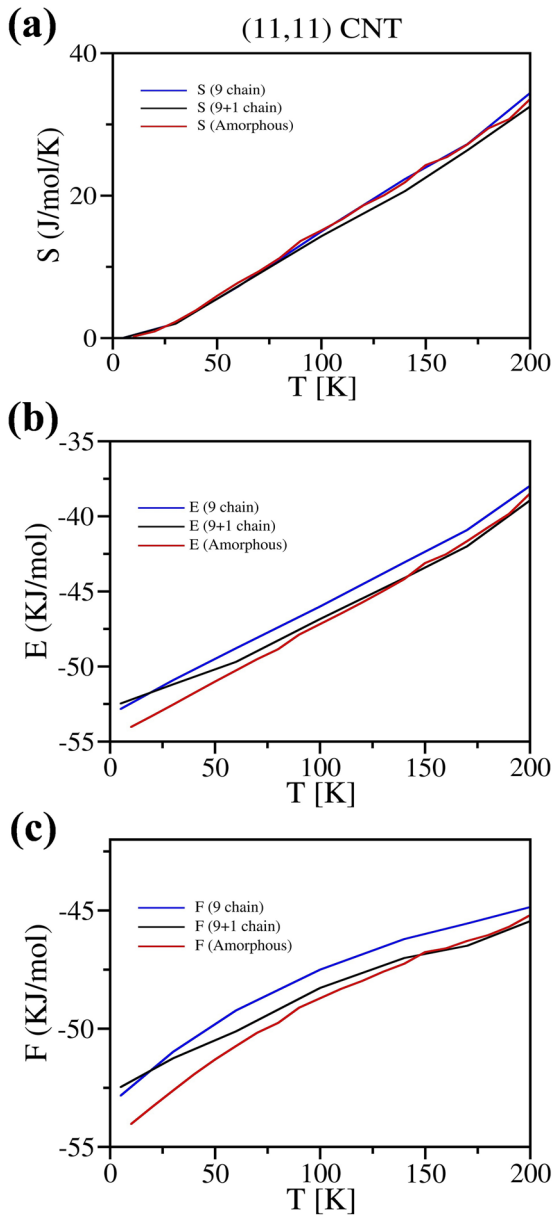

FIG. 9. (a) Entropy, (b) enthalpy, and (c) free energy for nonagon ice (9 chain) and nonagon ice with a central chain (9+1 chain) confined inside the (11,11) CNT reveals that the latter one is more stable than the former. However, the free energy calculation reveals that the amorphous phase is the most stable phase in the (11,11) CNT below 150 K.

$$\mathrm{CDF} = \frac{\rho(r_{xy})}{\rho}, \tag{19}$$

where $\rho(r_{xy})$ is the areal density in the XY plane and ρ is the total density of water confined inside a CNT. We also calculated

$$g_{o-o}(z) = \frac{1}{N(L-z)} \sum_{i=1}^{N} \sum_{j=1, j\neq i}^{N} \delta(z - z_{ij}), \tag{20}$$

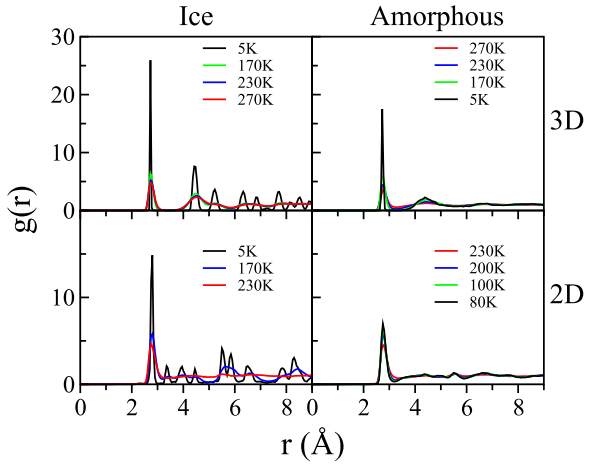

FIG. 10. Radial distribution function (RDF) for bulk phases (upper panel) and 2D confined phases (lower panel). Red to black and vice versa denote the change in temperature while cooling and heating protocols.

where $g_{o-o}(z)$ is the oxygen–oxygen pair correlation function of confined water inside a L = 40 Å long CNT, N is the total number of molecules confined inside a CNT, and z_{ij} is the difference in the z-coordinate of the ith and jth molecules.

We find that for the nonagon ice structure inside the (11,11) CNT (upper panel of Fig. 11), the CDF reveals a single peak at ~4 Å up to 100 K with a weak axial peak 0.5 Å emerging above 100 K. Due to the near constant density in these systems, this result indicates a splitting of the distribution of the H_2O molecules above 100 K, with increased molecular density near the central axis of the CNT. We also find that as the temperature increases, the ~4 Å main peak becomes smaller and shifts toward the central axis due to the interactions with the axial peak. Indeed, the final resulting structure mimics that of the nonagon ice motif with a central chain (middle

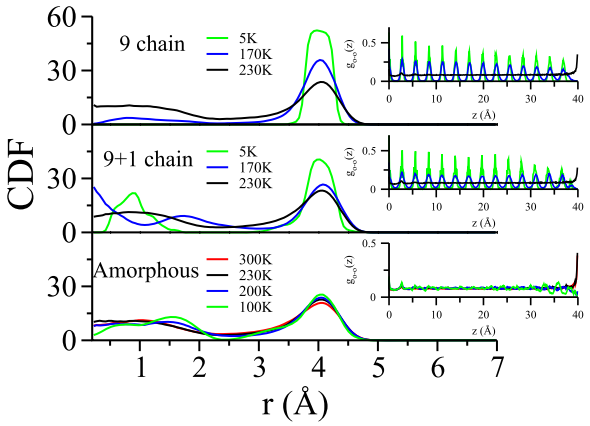

FIG. 11. Cylindrical distribution function (CDF) [defined in Eq. (19)] for nonagon ice (upper panel), nonagon ice with a central chain (middle panel), and the amorphous phase (lower panel) of confined water inside the (11,11) CNT. The two-point correlation function [defined in Eq. (20)] plotted in the z direction, which is the direction of the CNT axis, reveals that water does not crystallize down to 100 K.

panel), albeit with lower intensity due to the reduced density. In the case of amorphous water inside the (11,11) CNT (lower panel of Fig. 11), we note that the CDF has two peaks at ~1 to 4 Å, and both peaks are not very well-separated, which suggests that the water molecule can move continuously laterally from the axis to the internal wall of the CNT. However, the peaks are separated at 100 K, which suggests that the water molecule cannot move from the axis to the internal wall due to the low kinetic energy to cross the free energy barrier along the radial direction. The pair correlation function, $g_{o-o}(z)$, in the z direction (along the CNT axis) reveals that the nonagon ice (upper panel of Fig. 11) and nonagon ice (middle panel of Fig. 11) with the central chain melts between 170 and 230 K. However, the amorphous phase (lower panel of Fig. 11) does not show any ordering until down to 100 K.

In summary, in the case of 1D and 2D water under nanoscale confinement, our calculations reveal that the entropy of the amorphous phase is greater than that of the corresponding ice structures. The entropy differences decrease slowly with temperature and cut the temperature axis around 0 K, which means that unlike the bulk system, the Kauzmann temperature of confined water, which signifies the glass transition temperature of confined water, lies at 0 K. This is consistent with the results of Berthier *et al.* who showed that there is a zero temperature glass transition for less than three dimensions.[60]

V. CONCLUSION

In this study, we explored the existence of a Kauzmann temperature for bulk water and water under nano-confinement of varying dimensionality. Specifically, we computed the entropy of 1D, 2D, and 3D phases and water in liquid and ice phases using the 2PT method. We showed that the results of our 3D calculations, employing the flexible TIP4P-2005 model, are in good agreement with those of the rigid TIP4P-2005 calculations of Saito *et al.*, for bulk ice-Ih and liquid, over the entire temperature range. More importantly, our calculated entropies clearly demonstrate that the Kauzmann temperature is present at 133 K, which is very close to the experimentally obtained glass transition temperature. However, for water under 2D and 1D nanoconfinement,[60,61] we found that the Kauzmann temperature is zero, implying that that there is no finite temperature glass transition for less than three dimensions.[60]

It is worth mentioning here that inferring low temperature properties of water and, in general, about glass forming liquids through computer simulations is challenging. Indeed, such liquids cannot be equilibrated at low temperatures in simulations carried out for time scales of the order of 1 μs. Using the relaxation time reported by Saito *et al.*,[22] we estimate that the lowest temperature at which we could equilibrate our bulk water system is about 150 K within 500 ns long simulation. This, however, does not prevent us from estimating the Kauzmann temperature. The standard procedure[5–7] used for estimating the Kauzmann temperature from simulations is to calculate the excess entropy ΔS at temperatures for which the liquid can be equilibrated over the time scale of the simulation and then extrapolate the results to lower temperatures to find the temperature at which the extrapolated value goes to zero.

There is another important point that we wish to highlight. Saito *et al.* used the TIP4P-2005 model to study equilibrium and dynamical properties of water at 1 atm pressure from MD simulations carried out for very long times (more than 50 μs at low temperatures).[22] They also used thermodynamic integration to calculate ΔS.[27] They reported the occurrence of a dynamical crossover at 220 K (interpreted as a fragile-strong crossover) and a Kauzmann temperature of 135 K.[27] These results are very similar to those reported here. In addition, the left panel of Fig. 6 shows that our results for ΔS at lower temperatures for which the system does not equilibrate during our 500 ns runs fall on the straight line fit of the data at higher temperatures. These observations suggest that the values of ΔS obtained from the velocity autocorrelation function (VACF) are fairly accurate even if the time at which the VACF is calculated is not long enough to attain equilibrium at the prevailing temperature. To check whether this is true, we calculated the VACF at 202 K, starting at three different times (10, 100, and 250 ns), after the time at which the temperature was set at this value. The relaxation time at this temperature is estimated to be ~50 ns. Hence, the system had not reached equilibrium in the calculation starting at 10 ns, and it must have reached equilibrium in the calculation that started at 250 ns. As shown in Fig. S1, the VACF calculated for these two starting times is essentially identical. Similar results were found for other temperatures. As shown in Table S1, the entropy values at 202 K obtained from the VACF using the 2PT method are essentially the same for the three values of the starting time. These results suggest that the value of the entropy obtained from the 2PT method is reliable even if the time at which the VACF is measured is not long enough for reaching full equilibration.

We also found that the difference in the fluidicity factors, a measure of anharmonicity in the 2PT method, is the main source of the difference in the entropy between two phases in any dimensions. However, further analysis of the translational fluidicity factor difference reveals that the Kauzmann temperature can also be calculated from the difference in the translational component of the fluidicity factor. It is worth noting that the fluidicity factor gives an accurate Kauzmann temperature when a frequency shift does not take place across the different phases of the material at the same temperature, and the major contribution in the excess entropy comes from the difference in the fluidicity factor.

SUPPLEMENTARY MATERIAL

See the supplementary material for the velocity autocorrelation and entropy values at different time intervals from a 250 ns long run at 202 K to show the equilibration and convergence of results.

ACKNOWLEDGMENTS

We acknowledge DST, India, for the computational support through TUE-CMS clusters, IISc, and SERC, IISc, for Cray SahasraT where most of the simulations were done. M.M. acknowledges the Council of Scientific and Industrial Research (CSIR), India, for financial support. C.D. acknowledges support from the SERB Distinguished Fellowship. S.S. acknowledges support through the J. C. Bose Fellowship (Grant No. SERB/F/2898/2015-16), SERB, DST, India.

DATA AVAILABILITY

The data that support the findings of this study are available from the corresponding author upon reasonable request.

REFERENCES

[1] J. S. Langer, "Theories of glass formation and the glass transition," Rep. Prog. Phys. **77**, 042501 (2014).
[2] M. D. Ediger and P. Harrowell, "Perspective: Supercooled liquids and glasses," J. Chem. Phys. **137**, 080901 (2012).
[3] A. Cavagna, "Supercooled liquids for pedestrians," Phys. Rep. **476**, 51–124 (2009).
[4] J. C. Dyre, "Colloquium: The glass transition and elastic models of glass-forming liquids," Rev. Mod. Phys. **78**, 953 (2006).
[5] P. G. Debenedetti and F. H. Stillinger, "Supercooled liquids and the glass transition," Nature **410**, 259–267 (2001).
[6] E. B. Moore and V. Molinero, "Ice crystallization in water's 'no-man's land'," J. Chem. Phys. **132**(24), 244504 (2010).
[7] S. Sastry, "Liquid limits: Glass transition and liquid-gas spinodal boundaries of metastable liquids," Phys. Rev. Lett. **85**(3), 590 (2000).
[8] A. Manka, H. Pathak, S. Tanimura, J. Wölk, R. Strey, and B. E. Wyslouzil, "Freezing water in no-man's land," Phys. Chem. Chem. Phys. **14**(13), 4505–4516 (2012).
[9] F. Smallenburg, L. Filion, and F. Sciortino, "Erasing no-man's land by thermodynamically stabilizing the liquid–liquid transition in tetrahedral particles," Nat. Phys. **10**(9), 653–657 (2014).
[10] O. Mishima and H. E. Stanley, "The relationship between liquid, supercooled and glassy water," Nature **396**(6709), 329–335 (1998).
[11] W. Kauzmann, "The nature of the glassy state and the behavior of liquids at low temperatures," Chem. Rev. **43**, 219–256 (1948).
[12] C. A. Angell, "Insights into phases of liquid water from study of its unusual glass-forming properties," Science **319**, 582–587 (2008).
[13] K. Ito, C. T. Moynihan, and C. A. Angell, "Thermodynamic determination of fragility in liquids and a fragile-to-strong liquid transition in water," Nature **398**(6727), 492–495 (1999).
[14] V. Velikov, S. Borick, and C. A. Angell, "The glass transition of water, based on hyperquenching experiments," Science **294**(5550), 2335–2338 (2001).
[15] Y. Yue and C. A. Angell, "Clarifying the glass-transition behaviour of water by comparison with hyperquenched inorganic glasses," Nature **427**(6976), 717–720 (2004).
[16] A. Hallbrucker, E. Mayer, and G. P. Johari, "Glass-liquid transition and the enthalpy of devitrification of annealed vapor-deposited amorphous solid water: A comparison with hyperquenched glassy water," J. Phys. Chem. **93**, 4986–4990 (1989).
[17] G. P. Johari, A. Hallbrucker, and E. Mayer, "The glass–liquid transition of hyperquenched water," Nature **330**, 552–553 (1987).
[18] A. Scala, F. W. Starr, E. La Nave, F. Sciortino, and H. E. Stanley, "Configurational entropy and diffusivity of supercooled water," Nature **406**(6792), 166–169 (2000).
[19] A. Faraone, L. Liu, C.-Y. Mou, C.-W. Yen, and S.-H. Chen, "Fragile-to-strong liquid transition in deeply supercooled confined water," J. Chem. Phys. **121**(22), 10843–10846 (2004).
[20] M. K. Rajasekaran and K. G. Ayappa, "Dynamical transitions of supercooled water in graphene oxide nanopores: Influence of surface hydrophilicity," J. Phys. Chem. B **124**, 4805 (2020).
[21] M. Rajasekaran and K. G. Ayappa, "Influence of surface hydrophilicity and hydration on the rotational relaxation of supercooled water on graphene oxide surfaces," Phys. Chem. Chem. Phys. **22**(28), 16080–16095 (2020).
[22] S. Saito, B. Bagchi, and I. Ohmine, "Crucial role of fragmented and isolated defects in persistent relaxation of deeply supercooled water," J. Chem. Phys. **149**, 124504 (2018).
[23] K. V. Agrawal, S. Shimizu, L. W. Drahushuk, D. Kilcoyne, and M. S. Strano, "Observation of extreme phase transition temperatures of water confined inside isolated carbon nanotubes," Nat. Nanotechnol. **12**, 267 (2017).
[24] H. Kumar, C. Dasgupta, and P. K. Maiti, "Phase transition in monolayer water confined in janus nanopore," Langmuir **34**, 12199–12205 (2018).
[25] J. L. F. Abascal and C. Vega, "A general purpose model for the condensed phases of water: TIP4P/2005," J. Chem. Phys. **123**, 234505 (2005).
[26] P. G. Debenedetti, F. Sciortino, and G. H. Zerze, "Second critical point in two realistic models of water," Science **369**(6501), 289–292 (2020).
[27] S. Saito and B. Bagchi, "Thermodynamic picture of vitrification of water through complex specific heat and entropy: A journey through 'no man's land'," J. Chem. Phys. **150**, 054502 (2019).
[28] G. Bussi, D. Donadio, and M. Parrinello, "Canonical sampling through velocity rescaling," J. Chem. Phys. **126**, 014101 (2007).
[29] H. L. Pi *et al.*, "Anomalies in water as obtained from computer simulations of the TIP4P/2005 model: Density maxima, and density, isothermal compressibility and heat capacity minima," Mol. Phys. **107**, 365–374 (2009).
[30] A. Saul and W. Wagner, "A fundamental equation for water covering the range from the melting line to 1273 K at pressures up to 25 000 MPa," J. Phys. Chem. Ref. Data **18**, 1537–1564 (1989).
[31] O. Byl *et al.*, "Unusual hydrogen bonding in water-filled carbon nanotubes," J. Am. Chem. Soc. **128**, 12090–12097 (2006).
[32] J. Bai, J. Wang, and X. C. Zeng, "Multiwalled ice helixes and ice nanotubes," Proc. Natl. Acad. Sci. U. S. A. **103**(52), 19664–19667 (2006).
[33] G. Reiter, J. C. Li, J. Mayers, T. Abdul-Redah, and P. Platzman, "The proton momentum distribution in water and ice," Braz. J. Phys. **34**, 142–147 (2004).
[34] K. Koga, G. T. Gao, H. Tanaka, and X. C. Zeng, "Formation of ordered ice nanotubes inside carbon nanotubes," Nature **412**, 802 (2001).
[35] B. Mukherjee, P. K. Maiti, C. Dasgupta, and A. K. Sood, "Strong correlations and Fickian water diffusion in narrow carbon nanotubes," J. Chem. Phys. **126**(12), 124704 (2007).
[36] B. Mukherjee, P. K. Maiti, C. Dasgupta, and A. K. Sood, "Strongly anisotropic orientational relaxation of water molecules in narrow carbon nanotubes and nanorings," ACS Nano **2**(6), 1189–1196 (2008).
[37] M. Moid, Y. Finkelstein, R. Moreh, and P. K. Maiti, "Microscopic study of proton kinetic energy anomaly for nanoconfined water," J. Phys. Chem. B **124**, 190–198 (2019).
[38] G. Algara-Siller *et al.*, "Square ice in graphene nanocapillaries," Nature **519**, 443–445 (2015).
[39] M. S. F. Mario, M. Neek-Amal, and F. Peeters, "AA-stacked bilayer square ice between graphene layers," Phys. Rev. B **92**, 245428 (2015).
[40] T. A. Pascal, C. P. Schwartz, K. V. Lawler, and D. Prendergast, "The purported square ice in bilayer graphene is a nanoscale, monolayer object," J. Chem. Phys. **150**, 231101 (2019).
[41] R. Srivastava, H. Docherty, J. K. Singh, and P. T. Cummings, "Phase transitions of water in graphite and mica pores," J. Phys. Chem. C **115**(25), 12448–12457 (2011).
[42] N. Raghav, S. Chakraborty, and P. K. Maiti, "Molecular mechanism of water permeation in a helium impermeable graphene and graphene oxide membrane," Phys. Chem. Chem. Phys. **17**, 20557–20562 (2015).
[43] S. Chakraborty, H. Kumar, C. Dasgupta, and P. K. Maiti, "Confined water: Structure, dynamics, and thermodynamics," Acc. Chem. Res. **50**, 2139–2146 (2017).
[44] S.-T. Lin, M. Blanco, and W. A. Goddard III, "The two-phase model for calculating thermodynamic properties of liquids from molecular dynamics: Validation for the phase diagram of Lennard-Jones fluids," J. Chem. Phys. **119**, 11792–11805 (2003).
[45] R. K. Pathria and P. D Beale, *Statistical Mechanics* (Academic Press, 2011).
[46] N. F. Carnahan and K. E. Starling, "Thermodynamic properties of a rigid-sphere fluid," J. Chem. Phys. **53**, 600–603 (1970).
[47] D. A. McQuarrie, *Statistical Mechanics* (Harper & Row, 1975).
[48] H. A. Eyring, *Comparison of the Ionization by and Stopping Power for Alpha Particles of Elements and Compounds* (University of California, 1927).
[49] M. A. González and J. L. F. Abascal, "A flexible model for water based on TIP4P/2005," J. Chem. Phys. **135**, 224516 (2011).
[50] J.-B. Brubach, A. Mermet, A. Filabozzi, A. Gerschel, and P. Roy, "Signatures of the hydrogen bonding in the infrared bands of water," J. Chem. Phys. **122**, 184509 (2005).
[51] T. A. Pascal, D. Schärf, Y. Jung, and T. D. Kühne, "On the absolute thermodynamics of from computer simulations: A comparison of first-principles molecular dynamics, reactive and empirical force fields," J. Chem. Phys. **137**, 244507 (2012).
[52] K. Amann-Winkel *et al.*, "Water's second glass transition," Proc. Natl. Acad. Sci. U. S. A. **110**, 17720–17725 (2013).

[53]Y. P. Handa and D. D. Klug, "Heat capacity and glass transition behavior of amorphous ice," J. Phys. Chem. **92**, 3323–3325 (1988).
[54]Y. Finkelstein and R. Moreh, "Proton dynamics in ice VII at high pressures," J. Chem. Phys. **139**, 044716 (2013).
[55]H. Pathak *et al.*, "Intermediate range O–O correlations in supercooled water down to 235 K," J. Chem. Phys. **150**, 224506 (2019).
[56]K. T. Wikfeldt, A. Nilsson, and L. G. M. Pettersson, "Spatially inhomogeneous bimodal inherent structure of simulated liquid water," Phys. Chem. Chem. Phys. **13**, 19918–19924 (2011).
[57]S. K. Reddy, D. R. Moberg, S. C. Straight, and F. Paesani, "Temperature-dependent vibrational spectra and structure of liquid water from classical and quantum simulations with the MB-pol potential energy function," J. Chem. Phys. **147**, 244504 (2017).
[58]E. A. Raymond, T. L. Tarbuck, and G. L. Richmond, "Isotopic dilution studies of the vapor/water interface as investigated by vibrational sum-frequency spectroscopy," J. Phys. Chem. B **106**, 2817–2820 (2002).
[59]Y. Liu, Q. Wang, T. Wu, and L. Zhang, "Fluid structure and transport properties of water inside carbon nanotubes," J. Chem. Phys. **123**, 234701 (2005).
[60]L. Berthier, P. Charbonneau, A. Ninarello, M. Ozawa, and S. Yaida, "Zero-temperature glass transition in two dimensions," Nat. Commun. **10**, 1508 (2019).
[61]L. Berthier, M. Ozawa, and C. Scalliet, "Configurational entropy of glass-forming liquids," J. Chem. Phys. **150**, 160902 (2019).
[62]S.-T. Lin, P. K. Maiti, and W. A. Goddard III, "Two-phase thermodynamic model for efficient and accurate absolute entropy of water from molecular dynamics simulations," J. Phys. Chem. B **114**(24), 8191–8198 (2010).